Article

Charge Separation versus Recombination in Dye-Sensitized Nanocrystalline Solar Cells: the Minimization of Kinetic Redundancy

Saif A. Haque, Emilio Palomares, Byung M. Cho, Alex N. M. Green, Narukuni Hirata, David R. Klug, and James R. Durrant

J. Am. Chem. Soc., **2005**, 127 (10), 3456-3462• DOI: 10.1021/ja0460357 • Publication Date (Web): 16 February 2005

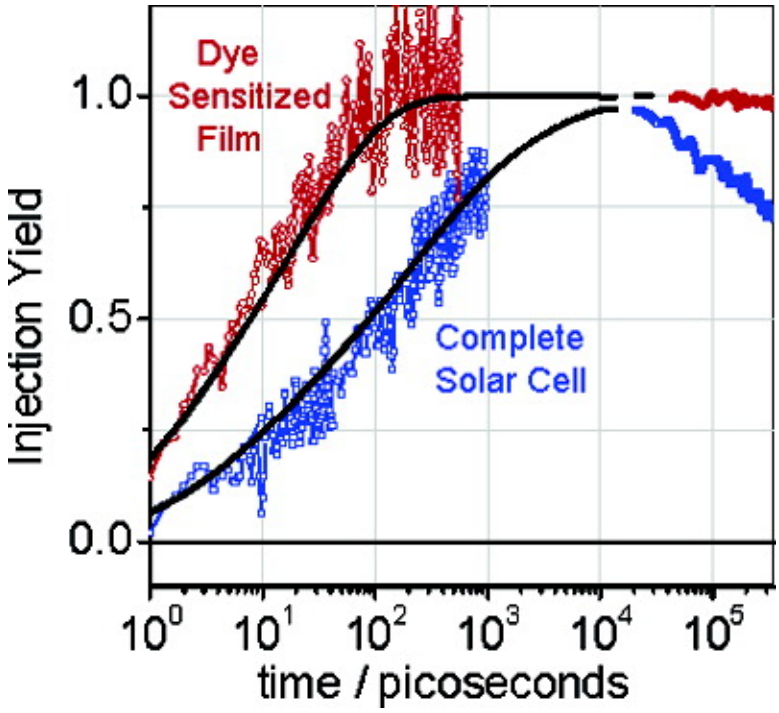

More About This Article

Additional resources and features associated with this article are available within the HTML version:

- Supporting Information
- Links to the 26 articles that cite this article, as of the time of this article download
- Access to high resolution figures
- Links to articles and content related to this article
- Copyright permission to reproduce figures and/or text from this article

J|A|C|S
ARTICLES
Published on Web 02/16/2005

Charge Separation versus Recombination in Dye-Sensitized Nanocrystalline Solar Cells: the Minimization of Kinetic Redundancy

Saif A. Haque,[†] Emilio Palomares,[†,§] Byung M. Cho,[‡] Alex N. M. Green,[†] Narukuni Hirata,[†] David R. Klug,[‡] and James R. Durrant*[,†]

Contribution from the Centre for Electronic Materials and Devices and Centre for Biological and Biophysical Science, Department of Chemistry, Imperial College London, Exhibition Road, South Kensington, London SW7 2AY, U.K., and Institut de Ciencia Molecular (IcMol), Universitat de Valencia, 46100-Burjassot, Valencia, Spain

Received July 3, 2004; E-mail: j.durrant@imperial.ac.uk

Abstract: In this paper we focus upon the electron injection dynamics in complete dye-sensitized nanocrystalline metal oxide solar cells (DSSCs). Electron injection dynamics are studied by transient absorption and emission studies of DSSCs and correlated with device photovoltaic performance and charge recombination dynamics. We find that the electron injection dynamics are dependent upon the composition of the redox electrolyte employed in the device. In a device with an electrolyte composition yielding optimum photovoltaic device efficiency, electron injection kinetics exhibit a half time of 150 ps. This half time is 20 times slower than that for control dye-sensitized films covered in inert organic liquids. This retardation is shown to result from the influence of the electrolyte upon the conduction band energetics of the TiO_2 electrode. We conclude that optimum DSSC device performance is obtained when the charge separation kinetics are just fast enough to compete successfully with the dye excited-state decay. These conditions allow a high injection yield while minimizing interfacial charge recombination losses, thereby minimizing "kinetic redundancy" in the device. We show furthermore that the nonexponential nature of the injection dynamics can be simulated by a simple inhomogeneous disorder model and discuss the relevance of our findings to the optimization of both dye-sensitized and polymer based photovoltaic devices.

Introduction

Photoinduced charge-transfer processes are of fundamental importance in many biological and chemical systems.[1,2] For example photoinduced charge separation employing molecular chromophores is the basis of natural plant photosynthesis. Emulation of this process in synthetic systems has been the subject of widespread study, including molecular donor−acceptor species in solution,[3] and a range of molecular-based films of interest for photovoltaic energy conversion, including dye-sensitized nanocrystalline metal oxides, and semiconducting polymer/fullerene blends.[4−6] In all cases, extensive studies have demonstrated that charge separation can occur on remarkably fast, subpicosecond time scales.[6−15] The observation of such ultrafast charge separation dynamics is widely accepted as a key milestone in establishing the viability of such molecular systems for efficient photochemical and photovoltaic energy conversion.

While the potential of achieving ultrafast charge separation in a range of molecular and molecular/inorganic systems is now well established, rather little attention has been placed on whether such dynamics are required, or indeed desirable, for efficient photovoltaic energy conversion. This issue has received attention for molecular donor/acceptor complexes in solution, where it is well established that careful control of the donor/acceptor electronic coupling is required to achieve a high charge

[†] Centre for Electronic Materials and Devices, Imperial College London.
[‡] Centre for Biological and Biophysical Science, Imperial College London.
[§] Universitat de Valencia.

(1) Bendal, D. S. Outline of theory of protein electron transfer. In *Protein electron transfer*; Moser, C. C.; Dutton, P. L., Eds.; BIOS Scientific Publishing: Chapter 1.
(2) Marcus, R. A.; Sutin, N. Electron transfers in chemistry and biology. *Biochim. Biophy. Acta* **1985**, *811*, 265−322
(3) Waiselewski, M. R. *Chem. Rev.* **1992**, *92*, 435−461
(4) Padinger, F.; Rittberger, R. S.; Sariciftci, N. S. *Adv. Funct. Mater*. **2003**, *13* (1), 85−88.
(5) Brabec, C. J.; Padinger, F.; Hummelen, J. C.; Janssen, R. A. J.; Sariciftci, N. S. *Synth. Met*. **1999**, *102* (1−3), pp 861−864.
(6) Hagfeldt, A.; Gratzel, M. *Chem. Rev.* **1995**, *95*, 49.
(7) Sariciftci, N. S.; Smilowitz, L.; Heeger, A. J.; Wudl, F. *Science* **1992**, *258* (5087), 1474−1476.
(8) Kraabel, B.; McBranch, D.; Lee, C. H.; Pakbaz, K.; Heeger, A. J.; Sandman, D. J. *Phys Rev B: Condens. Matter* **1994**, *50* (24), 18543−18552.
(9) Tachibana, Y.; Moser, J. E.; Gratzel, M.; Klug, D. R.; Durrant, J. R. *J. Phys. Chem.* **1996**, *100* (51), 20056.
(10) Hannappel, T. Burfeindt, B.; Storck, W.; Willig, F. *J. Phys. Chem. B* **1997**, *101*, 6799−6802.
(11) Benko, G. Kallioinen, J.; Korppi-Tommola, J. E. I.; Yartsev, A. P.; Sundstrom, V. *J. Am. Chem. Soc*. **2002**, *124*, 3, 489−493.
(12) Benko, G.; Kallioinen, J. T.; Myllyperkio, P.; Trif, F.; Korppi-Tommola, J. R. I.; Yartsev, A. P.; Sundstrom, V. *J. Phys. Chem. B* **2004**, *108* (9), 2862−2867.
(13) Schnadt, J.; Bruhwiler, P. A.; Patthey, L.; O'Shea, J. N.; Sodergren, S.; Odelius, M.; Ahuja, R.; Karis, O.; Bassler, M.; Persson, P.; Siegbahn, H.; Lunell, S.; Martensson, N. *Nature* **2002**, *418*, 620−623.
(14) Stier, W.; Duncan, W. R.; Prezhdo, O. V. *Adv. Mater*. **2004**, *16* (3), 240−244.
(15) Ashbury, J.; Hao, E.; Wang, Y.; Ghosh, H. N.; Lian, T. *J. Phys. Chem. B* **2001**, *105*, 4545−4557.

10.1021/ja0460357 CCC: $30.25

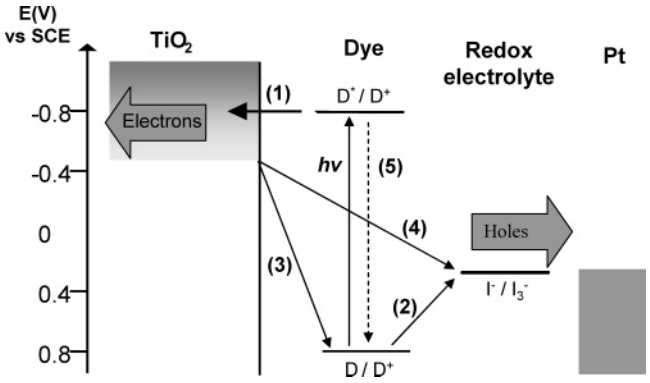

Figure 1. Schematic diagram showing different components in a dye-sensitized nanocrystalline semiconductor solar cell: a $(Bu_4N)_2Ru(dcbpy)_2(NCS)_2$-sensitized nanocrystalline TiO_2 film, interpenetrated by a liquid-based I^-/I_2 redox electrolyte containing lithium salts and 4-*tert*-butyl pyridine additives. Also shown are the different electron transfer processes in the solar cell: electron injection from dye excited state into the conduction band of TiO_2 semiconductor (1); regeneration of the dye cation by electron transfer from the redox couple (2); charge recombination to the cation of the dye (3); recombination to the redox couple (4); and excited state decay to ground (5).

separation yield while at the same time minimizing the rate of the subsequent charge recombination.[16] However, for photovoltaic materials, the correlation between charge separation dynamics and device performance has not been directly addressed, with ultrafast studies of charge separation dynamics typically employing isolated photoactive layers rather than complete devices.

We report here a study of the charge separation dynamics in complete dye-sensitized semiconductor solar cells (DSSCs) as a function of device composition. The most efficient DSSCs are currently based upon a ruthenium dye-sensitized nanocrystalline TiO_2 film interpenetrated by a hole-transporting material (HTM) comprising liquid electrolyte containing an iodine/iodide redox couple.[17] Such devices are currently attracting extensive scientific and tehnological interest. The operation of such a device is illustrated in Figure 1. Visible light is absorbed by the sensitizer dye, typically $[RuL_2(NCS)_2]$ (L = 4,4′-dicarboxy-2,2′-bipyridyl). Electron injection from the excited state of the dye into the conduction band of the TiO_2 (1) is followed by subsequent regeneration of the dye by electron donation from an I^-/I_3^- redox couple. The photoinjected electrons in the TiO_2 have two possible recombination pathways: direct recombination with the oxidized dye (3) or with the redox couple (4).

A number of recent spectroscopic studies have addressed the electron injection reaction in dye-sensitized nanocrystalline TiO_2 films in air or covered inactive organic solvents. Such studies have generally reported ultrafast injection kinetics on subpicosecond time scales.[6−11,13−15] with some reports, including our own, indicating that these dynamics are multiexponential extending up to tens of picoseconds.[12,18−23] In contrast, the excited-state lifetime for the isolated $RuL_2(NCS)_2$ sensitizer dye in degassed solution has been reported as 50 ns, indicating that charge separation dynamics as slow as 1 ns should be sufficient to yield a high charge separation yield. In this regard we reported recently a study addressing the influence of dye protonation upon the charge separation dynamics of $RuL_2(NCS)_2/TiO_2$ films.[18] Previous studies had shown that the di-tetrabutylammonium (di-TBA) salt of this dye (widely referred to as "N719") exhibited a superior photovoltaic device performance to that of fully protonated dye "N3".[33] Our study found that the partially deprotonated N719 dye exhibited an order of magnitude slower charge separation dynamics than the fully protonated "N3" dye, with charge separation half-times of 12 and 0.4 ps for the N719 and N3 dyes, respectively. It is apparent from this study that the dye yielding the superior photovoltaic device performance, namely N719, exhibited slower charge separation dynamics. The enhancement in device performance for the N719 dye was attributed rather to reduced charge recombination losses resulting from the influence of dye protons upon the energetics of nanocrystalline TiO_2.[18] In this study, as in previous reports, the ultrafast studies were conducted on isolated dye-sensitized films rather than complete devices, complicating direct correlation of the injection dynamics with device performance. However this study clearly suggests that subpicosecond injection dynamics may indeed not be necessary for optimum device performance.

We report herein a study of the correlation between the electron injection dynamics and device performance in complete DSSC. More specifically we have employed ultrafast optical pump−probe, time-resolved emission, and millisecond transient absorption spectroscopies to study both the charge separation and recombination dynamics in complete DSSCs as a function of redox electrolyte composition. To address the correlation between electron dynamics and device performance, we have studied devices employing three different redox electrolytes. Our study used an "optimized" electrolyte including both lithium ions and 4-*tert*-butyl pyridine additives which gives the highest device photovoltaic performance and two control electrolytes in which one or other additive was omitted, which both give lower device performances. These additives are commonly employed to enhance the photovoltaic performance of DSSCs, with the Li salts being added to improve device short circuit current I_{sc} and the 4-*tert*-butyl pyridine being added to improve device open circuit voltage V_{oc}. In this paper we find that both dynamics of charge separation and charge recombination are

(16) Davis, W. B.; Svec, W. A.; Ratner, M. A.; Wasielewski, M. R. *Nature* **1998**, *396*, 60−63.
(17) Hagfeldt, A.; Gratzel, M. *Acc. Chem Res*. **2000**, *33*, 269−277.
(18) Tachibana, Y.; Nazeeruddin, M. K.; Gratzel, M.; Klug, D. R.; Durrant, J. R. *Chem. Phys.* **2002**, *285*, 127−132.
(19) Tachibana, Y.; Haque, S. A.; Mercer, I. P.; Moser, J. E.; Klug, D. R.; Durrant, J. R. *J. Phys. Chem. B* **2001**, *105*, 7424−7431.
(20) Tachibana, Y.; Haque, S. A.; Mercer, I. P.; Klug, D. R.; Durrant, J. R. *J. Phys. Chem. B* **2000**, *104*, 1198−1205.
(21) Kallioinen, J.; Lehtovuori, V.; Myllyperkio, P.; Korppi-Tommola, J. E. I. *Chem. Phys. Lett.* **2001**, *340*, 217−221.
(22) Tachibana, Y.; Rubstov, I. V.; Montanari, I.; Yoshihara, K.; Klug, D. R.; Durrant, J. R. *J. Photochem. Photobiol., A* **2001**, *142*, 215−220.
(23) Durrant, J. R.; *J. Photochem. Photobiol., A* **2002**, *148*, 5−10.
(24) Barbe, C. J.; Arendse, F.; Comte, P.; Jirousek, M.; Lenzmann, F.; Shklover, V.; Gratzel, M. *J. Am. Ceram. Soc.* **1997**, *80* (12), 3157−3171.
(25) Palomares, E.; Clifford, J. N.; Haque, S. A.; Lutz, T.; Durrant, J. R. *J. Am. Chem. Soc*. **2003**, *125*, 475−482
(26) Spath, M.; Sommeling, P. M.; van Roosmalen, J. A. M.; Smit, H. J. P.; van der Burg, N. P. G.; Mahieu, D. R.; Bakker, N. J.; Kroon, J. M. *Prog. Photovoltaics* **2003**. *11*, 207.
(27) Cho, B. M. Protein Dynamics Measured by Non-Linear Spectroscopy, Ph.D. Thesis, University of London.
(28) Nogueira, A. F.; Montanari, I.; Nelson, J.; Winder, C.; Sariciftci, N. S.; Brabec, C.; Durrant, J. R. *J. Phys. Chem. B* **2003**, *107*, 1567−1573.
(29) Green, A. N. M.; Palomares, E.; Durrant, J. R. In preparation.
(30) Nazeeruddin, M. K.; Kay, A.; Rodicio, I.; Humphrey-Baker, R.; Muller, E.; Liska, P.; Vlachopolous, N.; Gratzel, M. *J. Am. Chem. Soc.* **1993**, *115*, 6382−6390.
(31) Haque, S. A.; Tachibana, Y.; Klug, D. R.; Durrant, J. R. *J. Phys. Chem. B* **1998**, *102*, 1745−1749.
(32) Montanari, I.; Nelson, J.; Durrant, J. R. *J. Phys. Chem. B*. **2002**, *106* (47), 12203−12210.
(33) Nazeeruddin, M. K.; Zakeeruddin, S. M.; Humphry-Baker, R.; Jirousek, M.; Liska, P.; Vlachopoulos, N.; Shklover, V.; Fischer, C. H.; Gratzel, M. *Inorg. Chem*. **1991**, *38*, 6298.

very sensitive to electrolyte composition. Optimum device performance is obtained when the electron injection rate is just fast enough to compete successfully with the decay of the dye excited state to ground.

Experimental Methods

Preparation of Dye Sensitized Solar Cells. Nanocrystalline titanium dioxide colloids were prepared as described in previously published methods and deposited using the doctor-blade technique on fluorine-doped tin oxide conducting glass (TEC 15, Hartford Glass).[24−26] The resulting mesoporous films consisted of TiO_2 particles approximately 15 nm in diameter and over 90% anatase as determined by Raman spectroscopy. With the exception of the device current/voltage characteristics shown in Figure 3a, all experiments employed 4 μm thickness, nonscattering films. For Figure 3a, devices were fabricated from 8 μm thickness films, with the addition of a 4 μm scattering overlayer. Sensitization of the photoelectrodes with the di-TBA salt of $RuL_2(NCS)_2$ (N719) was achieved by immersing the electrodes in a 1mM solution of dye in 1:1 acetonitrile/*tert*-butyl alcohol overnight, followed by rinsing in ethanol to remove unadsorbed dye.

Transparent counter electrodes were prepared by chemically depositing platinum from 0.05 M hexachloroplatanic acid in 2-propanol on to a second slide of conducting glass. Sandwich cells (1 cm^2) were then prepared by sealing together the TiO_2 coated electrode with the counter electrode using a transparent film of Surlyn 1472 polymer (DuPont Ltd.) at 110 °C. The electrolyte was then introduced through holes drilled in the counter electrode, which were sealed immediately with microscope cover slides and additional strips of Surlyn to avoid leakage unless otherwise stated. Experiments employed three different redox electrolytes:

(1) Electrolyte A: 0.6 M tetrabutylammonium iodide, 0.1 M lithium iodide, 0.5 M 4-*tert*-butylpyridine, and 100 mM iodine dissolved in acetonitrile (HPLC grade, Fluka).

(2) Electrolyte B: same as electrolyte A but omitting the LiI.

(3) Electrolyte C: same as electrolyte A but omitting the 4-*tert*-butylpyridine.

Device Characterization. Current−voltage measurements were obtained using with a ScienceTech solar simulator and AM 1.5 spectral filter. Calibration of the light intensity was achieved by using band-pass filters of known transmission combined with a silicon photodiode with independently certified spectral response, calibrated at the ISE-Fraunhofer Insitut in Freiburg Germany. The lamp intensity was adjusted to give close (±5%) agreement with theoretical one sun AM 1.5 intensity over the spectral region of the dye optical absorption (450−700 nm).

Transient Spectroscopies. Details of our pump−probe transient absorption spectrometer will be detailed elsewhere.[27].Samples were excited with a pulse energy of ∼30 nJ (0.38 mJ/cm^{-2}, 5 kHz) at 620 nm corresponding to $\leq 1.5 \pm 0.5$ electron per particle per excitation pulse. Experiments were conducted with samples rotated at a sufficient speed so that the sample area was replaced every 3 ms, thereby avoiding degradation or charge buildup within sample. The instrument response (10∼90% rise time of the transient absorption signal) of the spectrometer was ∼250 fs determined by a dye standard of Nile Blue in methanol for a probe wavelength of 800 nm. Data were collected on time scales of 0−50 ps and 0−900 ps. Considerable care was taken to ensure that experiments employed matched densities of absorbed photons. For the ZrO_2 control data, lower dye loadings were used, with the data being correspondingly normalized by the film optical density at the excitation wavelength to allow quantitative comparison with the TiO_2 film data. Nanosecond transient absorption data were collected as previously.[28]

Charge recombination dynamics were monitored by employing a pulsed voltage excitation source, and optical absorbance data collection. A fixed voltage (set at 550 mV) was applied across the cell for 1 s, resulting in increased electron occupancy of the photoelectrode. The cell was then switched to open circuit, and the subsequent recombination of the TiO_2 electrons with the redox couple was monitored by decay of the electron optical absorbance at 1000 nm. A more in-depth analysis of this technique will be presented elsewhere.[29]

Transient emission data were collected using 635 nm excitation from a IBH NanoLED-06 pulsed laser diode (repetition rate 1 MHz, pulse duration 0.2 ns, intensity ∼1 mW/cm^2. Emission was collected at 750 nm (bandwidth 50 nm) using a microchannel plate, with an instrument response of ∼200 ps. Data were collected for matched data collection times of 2500 s.

Results

We consider first pump−probe studies of photoinduced electron injection in a complete DSSC with electrolyte A. The electron injection dynamics were monitored, as previously, by time-resolving the appearance of the dye cation absorption band at 800 nm,[9,18] as shown in Figure 2a. Also shown in this figure are control data taken for dye-sensitized TiO_2 and ZrO_2 films covered in inert organic solvent (50:50 propylene carbonate/ethylene carbonate). These control data are almost indistinguishable from those we have reported previously for this sensitizer dye/metal oxide combination.[18] The data collected for the dye-sensitized ZrO_2 film (see insert to Figure 2a) correspond to the absorbance increase of the dye excited-state alone, as for this electrode the high metal oxide conduction band edge precludes significant electron injection. All samples showed an instrument response limited initial rise assigned from comparison to the ZrO_2 control data, as previously,[9] primarily to dye excited state formation. The magnitude of this initial increase is similar for both the DSSC and ZrO_2 control samples, indicating negligible (<10%) electron injection in the DSSC within our instrument response (<250 fs). Following this initial rise, it is apparent that the subsequent signal increase, assigned to grow-in of dye cation absorption due to charge separation, is much slower for the DSSC relative to the control dye-sensitized TiO_2 film, indicative of slower electron injection dynamics for the DSSC relative to the control dye-sensitized TiO_2 film covered in redox inactive solvent.

Time correlated single photon counting studies were employed to provide further evidence for a significant retardation of the electron injection dynamics in the DSSC compared to the control sample. Typical data are shown in Figure 2c. It is apparent that the excited state decay dynamics are strongly retarded for the DSSC compared to the control sample, in good agreement with the transient absorption data shown in Figure 2a.

It is apparent from the data shown in Figure 2a and c that the dye cation formation dynamics, and the concomitant excited state decay dynamics, are highly dispersive, proceeding over a broad range of time scales. The observation of such dispersive injection dynamics is consistent with our previous studies where we reported multiexponential electron injection kinetics for a variety of sensitizer dyes anchored onto nanocrystalline TiO_2 films.[18,19,22] In the presence of such dispersive dynamics, direct comparison of the electron injection dynamics for the DSSC and the control dye-sensitized TiO_2 film can be most readily made by consideration of data shown on a logarithmic time scale, as shown in Figure 2b. To further facilitate comparison of the data shown in this figure, contributions to the transient absorption signal from dye excited-state absorption have been subtracted by reference to data collected for the dye/ZrO_2 control

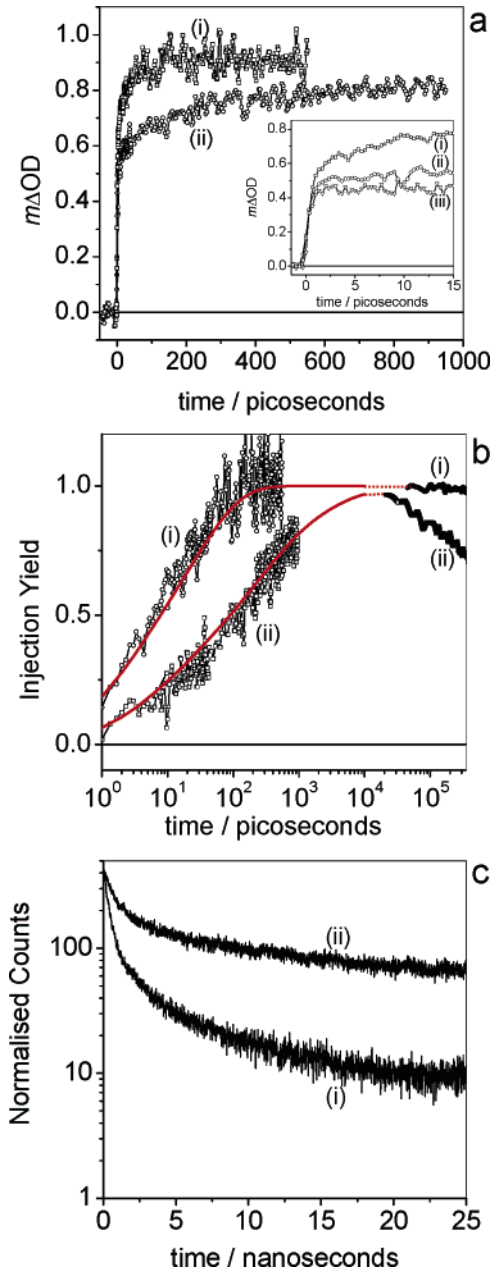

Figure 2. (a) Picosecond transient absorption data obtained for a $(Bu_4N)_2$-$Ru(dcbpy)_2(NCS)_2$-sensitized TiO_2 film (2a(i)) and for a complete solar cell (2a(ii)). Data shown here were collected at a probe wavelength of 800 nm following 610 nm excitation. The insert to part a shows transient absorption data on faster time scales with the addition of control data (iii) obtained with a dye-coated noninjecting ZrO_2 film. (b) Comparison of electron injection dynamics for the dye-coated TiO_2 electrode (2b(i)) and complete solar cell (2b(ii)). These data were obtained by subtracting the contribution of dye excited-state absorption from the data shown in part a. Data are plotted on a logarithmic time scale with the additional data collected on nanosecond time scales. Smooth lines show Monte Carlo simulations of these data employing eq 1; fit parameters from these simulations are given in Table 1. (c) Corresponding time-resolved single photon counting decays for the same samples, showing the dye excited state emission decay dynamics on the nanosecond time scale.

film, resulting in the signal amplitude being directly proportional to the density of dye cations and, therefore, to the yield of electron injection.

The electron injection dynamics shown in Figure 2b can be most readily quanitified by consideration of the half-time for electron injection, $t_{50\%}$, which corresponds to 8 ± 2 and 150 ± 50 ps for the dye-coated TiO_2 control film and complete DSSC, respectively. We thus conclude that the complete solar cell exhibits an ~20-fold retardation in the rate of electron injection with respect to the dye-sensitized TiO_2 electrode covered in inert solvent. We note that this 150 ps half-time for electron injection in the solar cell is still fast compared to excited state decay to ground (~50 ns),[30] consistent with efficient electron injection for both samples.

Further analysis of the yield of electron injection for the two TiO_2 samples studied in Figure 2 was obtained by transient absorption data collected on the nanosecond time scale, also included in Figure 2b. For the dye-sensitized TiO_2 film, a long-lived transient signal is observed, consistent with the microsecond−millisecond recombination dynamics we have reported previously for such samples.[9] For the DSSC, this transient signal is observed to decay with a half-time of ~1 μs, assigned to dye cation rereduction by the redox electrolyte, as we have reported previously.[31,32] For ease of viewing, dashed lines extrapolate between the data collected on the two time scales. It is apparent that the initial nanosecond signal magnitudes for both samples are similar (1:0.95 ± 0.05 for the dye-sensitized film and DSSC, respectively), consistent with similar electron yields for both samples.

It is also apparent from the data shown in Figure 2 that the injection dynamics are highly dispersive, extending over several orders of magnitude in time scale, consistent with our previous observations of dye-sensitized TiO_2 films. This dispersion is particularly evident for the DSSC, with a significant proportion (~10%) occurring on time scales > 1 ns. We have previously modeled this dispersive behavior employing a Zn porphyrin sensitizer dye.[22] This model is based upon local inhomogeneities in the electron injection energetics. Assuming an exponentially increasing density of TiO_2 acceptor states $g(E) \propto \exp(-E/E_0)$,[23] such energetic inhomogeneities have the effect of resulting in variations in the density of acceptor states for activationless electron injection and therefore in the integrated electronic coupling for this reaction, thereby resulting in a distribution of electron injection rate constants. Employing this model, and assuming a Gaussian distribution of energy offsets d_i with fwhm Δ, the microscopic injection rate constant $k(d_i)$ for energy offset d_i is given by[22]

$$k(d_i) = k(0)\frac{V^2(d_i)}{V^2(0)} = k(0)\exp\left(\frac{2d_i}{E_0}\right) \qquad (1)$$

Using this simple model, Monte Carlo numerical calculations were employed to simulate the experimentally observed reaction dynamics, as shown by the smooth lines in Figure 2b. It is apparent that these simulations are in excellent agreement with the experimental data. This agreement is particularly noteworthy as these simulations are dependent upon only two parameters, the value $k(0)$, corresponding to the injection kinetics with mean reaction free energy, and the ratio Δ/E_0; the values for these two parameters obtained from the simulations are shown in Table 1. The value for $k(0)$ is 16 times smaller for the DSSC relative to the dye-sensitized film, consistent with the slower electron injection dynamics. The ratio Δ/E_0 for the dye-sensitized film is similar to what we have reported previously for Zn porphyrin sensitized TiO_2 films; using a value for E_0 of 100 meV, [22,23] this corresponds to a fwhm for the energetic

Table 1. Parameters for the Monte Carlo Simulations Employing Eq 1 Used to Determine Best Fit Traces to the Absorption Transients Shown in Figure 2b

	film	solar cell
$k(0)/s^{-1}$	8×10^{10}	5×10^{9}
Δ/E_0	1.9	3.7

disorder of 190 meV. For the DSSC, the ratio is twice as big; as similar values of E_0 have been reported for both TiO_2 films and complete devices, the larger ratio is most probably indicative of a greater degree of energetic disorder within the DSSC relative to the dye-sensitized films alone.

We now consider the correlation between electron injection dynamics and device photovoltaic performance. To this end we compare data for DSSCs employing the different electrolytes A, B, and C as shown in Figure 3. Figure 3a−c show, respectively, the current−voltage data in the dark and under AM1.5 illumination, the time-resolved emission decay profiles, and charge recombination decays for DSSCs employing the three electrolytes. Emission decay data were collected for matched densities of absorbed photons, allowing quantitative comparison of signal amplitude. It is apparent that the omission of 4-*tert*-butyl pyridine, electrolyte C, results in lower amplitude and more rapidly decaying emission data relative to electrolyte A, indicative of faster electron injection dynamics. This is however at the expense of a larger dark current and faster recombination kinetics, and thereby a lower device V_{oc} and energy conversion efficiency. For electrolyte C, the emission decay dynamics are similar to those obtained from dye-sensitized TiO_2 films covered only in inert solvent. Conversely omission of lithium ions from the electrolyte (electrolyte B) results in higher amplitude and slower emission decay dynamics, indicative of slower injection dynamics, but a lower dark current and slower recombination losses. In this case, the cell exhibits a significantly lower I_{sc}, consistent with the slower injection dynamics no longer competing successfully with dye excited state decay to ground and resulting in significant loss of device performance. Optimum device performance is obtained when both lithium ions and 4-*tert*-butyl pyridine are added to the redox electrolyte.

Discussion

Previous studies of dye-sensitized nanocrystalline metal oxide films have demonstrated that electron injection dynamics can proceed on remarkably fast time scales, in some cases <100 fs.[6−15] In contrast the dynamics we report here for a complete DSSC in the presence of an "optimized" electrolyte appear strikingly slow, with a reaction half-time of only 150 ps. This observation raises two obvious questions, namely the mechanism which results in such slow injection dynamics for the DSSC and whether such slow injection dynamics are incidental to optimized device photovoltaic performance.

We will first of all consider the mechanism by which the electron injection dynamics in the DSSC are slow relative to most previous studies of dye-sensitized TiO_2 films. We note that even for the control dye-sensitized film covered in inert organic solvent, the dynamics are slow compared to most previous studies.[9,10,11,15] This can be attributed to the use in these control data of the partially de-protonated $RuL_2(NCS)_2$ sensitizer dye "N719". This sensitizer dye results in an order of magnitude retardation of the injection dynamics relative to the more widely studied fully protonated dye "N3", as we have reported previously.[18] We note that this deprotonated dye was selected for this study due to its superior performance in terms of efficiency of the resulting DSSC.[33] However, in addition to this influence of the sensitizer dye, it is apparent that the complete DSSC results in a further order of magnitude retardation of the injection dynamics relative to the control data for films covered in organic solvent. Comparison of the data collected with different electrolytes clearly indicates that this retardation primarily results from interaction of the electrolyte with the dye-sensitized film. In particular it is apparent that omission of *tert*-butyl pyridine from the electrolyte results in excited-state decay dynamics for the complete DSSC which are similar to those obtained for the control film data, indicating that this component of the electrolyte plays a key role in the retardation of the injection dynamics observed in the complete DSSC with "optimized" electrolyte composition.

We have previously proposed that the retardation of the injection dynamics observed for the partially deprotonated $RuL_2(NCS)_2$ relative to the fully protonated dye results from the influence of the sensitizer dye protons on the energetics of electron acceptor states in the TiO_2.[34,35] This proposition is consistent with the well-known Nernstein dependence of the conduction band of nanocrystalline TiO_2 films upon pH. Similarly, we have shown that the immersion of dye-sensitized TiO_2 electrodes in redox-inactive electrolytes in the presence or absence of lithium ions can result in an order of magnitude acceleration of the dynamics of electron injection. This observation was also interpreted in terms of the well established influence of lithium ions upon the TiO_2 conduction band energetics. Furthermore our previous spectroelectrochemical studies have shown that pyridine functions as a base within the electrolyte, shifting the TiO_2 conduction band to more negative potentials.[36] We thus conclude that the slow electron injection dynamics we report here for a DSSC with optimized electrolyte composition primarily result from influence of this electrolyte upon the energetics of the TiO_2 conduction band, with the electrolyte resulting in a shift of the conduction band to more negative potentials relative to the control data for the film covered in inert solvent. This negative shift reduces the density of acceptor states available for electron injection and, thereby, retards the kinetics of electron injection.

We turn now to consideration of the extent to which the dynamics we report can be considered "optimum". Efficient operation of DSSC requires the photogeneration of a high yield of a long-lived interfacial charge separated state. Analogous photoinduced charge separation dynamics have been extensively studied in homogeneous supermolecular structures, such as donor/acceptor diads suspended in solution.[37−39] Such studies have shown that the dynamics of charge separation and recombination are closely related, with for example modulation

(34) Redmond, G.; Fitzmaurice, D.; Gratzel, M. *J. Phys. Chem.* **1993**, *97*, 6951−6954.
(35) Rothenberger, G.; Fitzmaurice, D.; Gratzel, M. *J. Phys. Chem.* **1992**, *96*, 5983−5986.
(36) Haque, S. A.; Tachibana, Y.; Willis, R. L.; Moser, J. E.; Gratzel, M.; Klug, D. R.; Durrant, J. R. *J. Phys. Chem. B* **2000**, *104*, 538−547.
(37) Fukozumi, S. *Org. Biomol. Chem.* **2003**, *1*, 609−620.
(38) Lomoth, R.; Haupl, T.; Johansson, O.; Hammarstrom, L. *Chem.—Eur. J.* **2002**, *8*, 102−110.
(39) Yamada, H.; Imahori, H.; Nishimura, Y.; Yamazaki, I.; Kyu, T. A.; Keun, S. K.; Kim, D.; Fukuzumi, S. *J. Am. Chem. Soc.* **2003**, *125*, 9129−9139

of the electronic coupling between the donor and acceptor having equal effects upon both the charge separation and recombination dynamics. Moreover variation of the energetics of charge separation results in modulation of not only the charge separation dynamics, but also modulation of recombination dynamics to both the diad ground and excited states. Optimization of molecular diad performance therefore requires careful consideration of all reaction dynamics, with for example "optimised" electronic coupling being a compromise between it being sufficiently large such that charge separation competes effectively with excited-state decay and it being sufficiently small to minimize charge recombination.

Such considerations can also be applied to the dye-sensitized TiO_2 interface. In this case the system is more complex due to the band of electron acceptor states in the TiO_2, resulting in more complex relationships between the reaction dynamics and their corresponding electronic coupling and energetics, as we have recently reviewed in detail. [40] However, it is clear that, from the data shown in Figure 3, at least for the changes in electrolyte composition addressed in this study, the kinetics of electron injection and recombination are closely correlated. This correlation can be understood in terms of the influence of the electrolyte upon the energetics of nanocrystalline TiO_2 electode, as illustrated in Figure 4. Omission of lithium ions from the electrolyte results in the negative shift of the TiO_2 conduction band energetics results in a reduction in a retardation of the electron injection dynamics, as we have reported previously,[19] but a lower electron occupancy at a given cell potential and, therefore, reduced recombination losses. The reverse effect is observed for the omission of *tert*-butylpyridine. Optimum photovoltaic performance is obtained when the electron injection kinetics are just sufficient to compete effectively with excited-state decay to ground; under these conditions near unity injection yield is obtained while minimizing recombination losses, in agreement with a recent "two level system" analysis of molecular cells.[41] These conditions can be regarded as minimizing kinetic redundancy within device function.

Comparison with our previous studies[36] suggests that the magnitude of the TiO_2 conduction band shifts associated with the variations in electrolyte composition employed in this study may be of the order of 300 meV. Using a value of E_0, the exponent of the TiO_2 density of states, of 100 meV, as discussed above, such band shifts would result in variations in the density of TiO_2 acceptor states of approximately $e^{300/100} \approx 20$, and therefore a variation in electron-transfer rate constants of $20^2 = 400$. Such variations in electron transfer rate constant are consistent with the electrolyte dependence of the transient emission data in Figure 3, which indicates an approximately 100 fold acceleration of the electron injection dynamics between electrolytes B and C. Similarly, conduction band shifts of this order are consistent with the 200 mV shift in the device open circuit voltage between these electrolytes.

In the study we report here, minimization of kinetic redundancy in the device is achieved by modulation of electrolyte composition. We note that several other strategies employed to optimize device performance can also be viewed as strategies designed to minimize kinetic redundancy in the device. These strategies include optimization of the sensitizer dye protonation, as discussed above, and the coating of the nanocrystalline TiO_2 film with metal oxide barrier layers, with the barrier layer thickness being optimized to still allow efficient electron injection while at the same time minimizing interfacial recombination dynamics.[25]

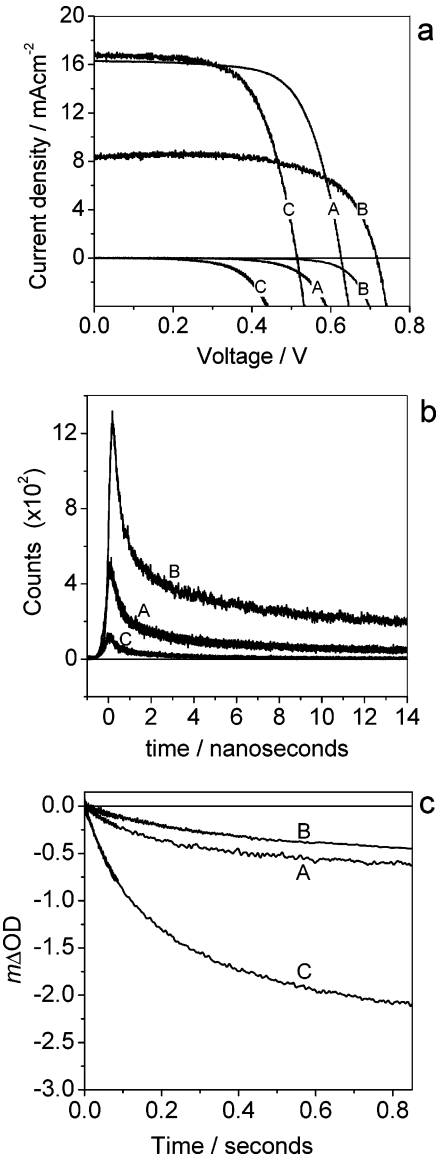

Figure 3. (a) Current−voltage characteristics for DSSCs employing three different electrolytes. Devices employed an acetonitrile-based I^-/I_2 redox electrolyte with lithium ions and 4-*tert*-butyl pyridine (A), with added 4-*tert*-butyl pyridine only (B), and with added lithium ions only (C). Device A shows optimum power conversion efficiency. (b) Corresponding time-resolved single photon counting decays of above devices A−C, respectively, normalized to the same number of photons absorbed. (c) Transient absorption data corresponding to TiO_2 electron population decay under open circuit conditions following the application of a 550 mV bias voltage. These decays are assigned to the charge recombination between the electrons in the TiO_2 and the redox electrolyte.

It can be concluded from the arguments detailed above that our observation of an electron injection half-time of ~150 ps is consistent with efficient device operation for this sensitizer dye and that the observation of faster injection dynamics would, in the absence of hot carrier collection processes, be indicative of a poorly optimized device. In this context, we note that electron injection from the short-lived (<100 fs), but more

(40) Durrant, J. R.; Haque, S. A.; Palomares, E. *Coord. Chem. Rev.* **2004**, *248* (13−14), 1247−1257.
(41) Nelson, J.; Kirkpatrick, J.; Ravirajan, P. *Phys. Rev. B* **2004**, *69* (3), 035337/1−035337/11.

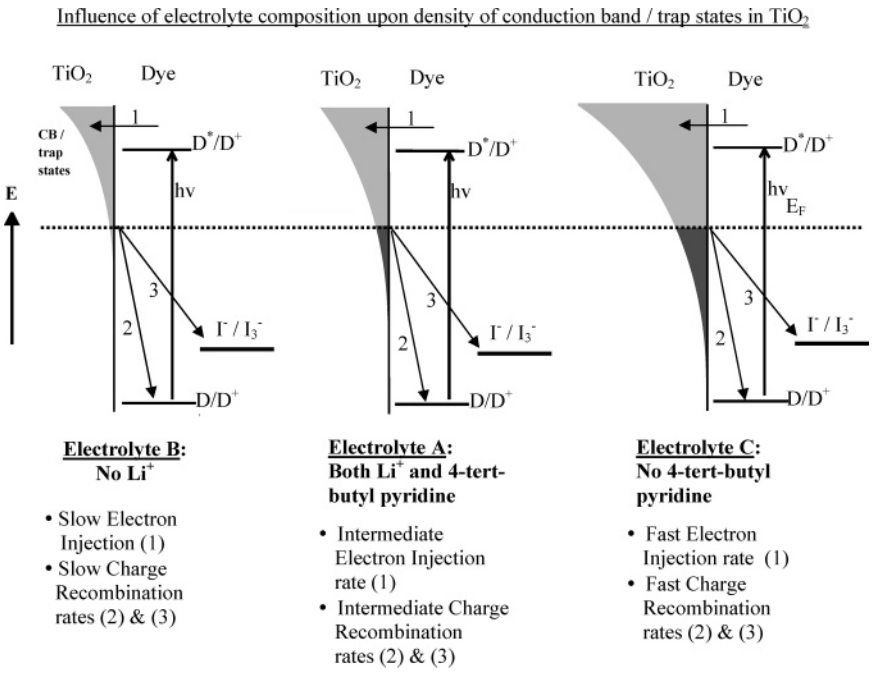

Figure 4. Schematic representation of electron injection (1) and charge recombination reactions (2 and 3) reactions at the TiO_2/dye/redox electrolyte interface in a DSSC as a function of electrolyte compostition. The variation in the electrolyte composition results in a shift of the conduction band/trap states in the nanocrystalline TiO_2 film, with the lithium ions shifting them to more positives potentials and 4-*tert*-butyl pyridine shifting them to more negative potentials.

energetic, singlet excited state of this dye[11] will be unlikely to contribute significantly to device function. We further note that arguments about kinetic redundancy are also likely to be applicable to other photovoltaic devices, such as polymer/C60 blends, in agreement with a recent theoretical analysis.[41] The recent observation of <50 fs charge separation dynamics in such a blend,[8] more than 3 orders of magnitude faster than excited state decay to ground, may be indicative of a system with significant kinetic redundancy caused by overly strong electronic coupling or mixing of the donor and acceptor species.

The achievement of "optimum" electron transfer dynamics in the DSSC is likely to be impeded significantly by the highly dispersive nature of these dynamics. Even for the "optimized" with an injection half-time of 150 ps, the dispersive nature of these dynamics results in the injection process only being 90% complete at 1 ns, with the remaining nanosecond injection dynamics starting having to compete with excited state decay to ground on the same time scale. As we have shown above, this dispersive behavior is consistent with local inhomogeneities in the electron injection kinetics, consistent with the disordered nature of the TiO_2 electrode. Such local inhomogeneities may be associated with local variations in surface protonation. Further discussion of this issue and its implication for future device optimization are given elsewhere.[40]

In summary we have addressed what the "optimum" charge separation dynamics are for optimum DSSC device function. Optimum device function, and specifically optimum device open circuit voltage, requires minimization of interfacial charge recombination. Such minimization however typically results in retardation of charge separation dynamics and, if taken too far, results in a loss of charge separation yield and therefore device short circuit current. As a result device optimization requires a suitable compromise between these two conflicting constraints. Consequently optimum device performance requires the avoidance of any "kinetic redundancy", with the charge separation dynamics being just fast enough to achieve a high yield of charge separation.

As such, the observation of an ultrafast, namely subpicosecond electron injection injection dynamics is an indicator of a poorly optimized device.

Acknowledgment. We are very pleased to acknowledge the EPSRC and the European Union (Contract Number: ENK6-CT-2001-00560 Nanomax) for financial support. E.P. would like to acknowledge the financial support from the European Union (Marie Curie European Fellowship Contract No. HPMF-CT-2002-0144). Supply of the $RuL_2(NCS)_2$ sensitizer dye from Johnson Matthey Ltd. and TiO_2 colloidal paste from the Energy Research Centre of The Netherlands (ECN), Department of Solar Energy is gratefully acknowledged. We would like to thank Chris Barnett for excellent technical support. The authors are also grateful to Francisco Fabregat-Santiago and Jenny Nelson for many helpful discussions.

JA0460357